amplify a 1.2-kb fragment. The probe used for Southern (DNA) blot hybridizations to verify targeted lines is a 2.1-kb Eco RI fragment from intron 1 located upstream of the sequences used in the construction of pEgfr-T2. The targeting frequency was 1/125.
15. R. W. Donaldson and C. W. Cohen, *Proc. Natl. Acad. Sci. U.S.A.* **89**, 8477 (1992).
16. Pieces of whole uteri containing implantation sites, placentas, and brains were fixed in 4% paraformaldehyde, embedded in paraffin, and 7-μm sections collected on glass slides before staining with hematoxylin-eosin (H&E) [R. Zeller, in *Cur. Prot. Mol. Biol.*, F. M. Ausabel *et al.*, Eds. (Wiley, New York, 1989), pp. 14.1.1–14.1.8]. Sections were hybridized with an ^{35}S-labeled antisense RNA probe made from a murine H19 complementary DNA (cDNA) [D. Sassoon and N. Rosenthal, in *Guide to Techniques in Mouse Development*, P. M. Wassarman and M. L. DePamphilis, Eds. (Academic Press, New York, 1993), pp. 384–404]. The slides were visualized with a Bio-Rad confocal microscope.
17. T. Tennenbaum *et al.*, *Cancer Res.* **52**, 2966 (1992).
18. We thank members of the Magnuson lab and B. Hogan for critical reading of the manuscript, C. Faust for help with confocal imaging, S. K. Dey, R. Schultz, D. L. Page, J. R. Goldenring, and D. Raiford for helpful discussions, and K. Newsom for technical assistance. We are indebted to S. Wert and J. Whitsett (University of Cincinnati) for help with immunohistochemical analyses and interpretation of lung histology. D.W.T. was supported by NIH grants HD07104 and GM14630. This work was supported by NIH grants HD26722 (T.M.), NS18381 (K.H.), CA46413 (R.J.C.), DK39261 (R.C.H.), and P30DK26657 (J.A.B.). R.J.C. and R.C.H. are VA Clinical Investigators. R.J.C. acknowledges support by the Joseph and Mary Keller Foundation.

10 April 1995; accepted 31 May 1995

Strain-Dependent Epithelial Defects in Mice Lacking the EGF Receptor

Maria Sibilia and Erwin F. Wagner

Mice and cells lacking the epidermal growth factor receptor (EGFR) were generated to examine its physiological role in vivo. Mutant fetuses are retarded in growth and die at mid-gestation in a 129/Sv genetic background, whereas in a 129/Sv × C57BL/6 cross some survive until birth and even to postnatal day 20 in a 129/Sv × C57BL/6 × MF1 background. Death in utero probably results from a defect in the spongiotrophoblast layer of the placenta. Newborn mutant mice have open eyes, rudimentary whiskers, immature lungs, and defects in the epidermis, correlating with the expression pattern of the EGFR as monitored by β-galactosidase activity. These defects are probably cell-autonomous because chimeric mice generated with EGFR$^{-/-}$ embryonic stem cells contribute small amounts of mutant cells to some organs. These results indicate that the EGFR regulates epithelial proliferation and differentiation and that the genetic background influences the resulting phenotype.

The EGFR (or *ERBB1*) belongs to a family of tyrosine kinase receptors (which includes *ERBB2/NEU*, *ERBB3*, and *ERBB4*) that show heterodimerization in vitro (*1*). Several ligands such as EGF, transforming growth factor–α (TGF-α), heparin-bound EGF, betacellulin, and amphiregulin can bind the EGFR and regulate many cellular processes (*1*). During mouse development, the receptor can be detected on the trophectoderm of the blastocyst and continues to be expressed together with several EGFR ligands in the placenta, uterus, and decidua (*2–4*). At mid-gestation, EGF binding activity can be detected in various organs, but only a few studies have localized the EGFR in specific tissues or cell types (*4*). In adult mice, the EGFR is expressed strongly in the liver and in tissues with regenerative epithelium, such as skin and gut (*4*). Amplification and overexpression of the EGFR has been detected in many human tumors of epithelial origin and in glioblastomas (*4*).

The gene encoding the EGFR was inactivated by replacement of part of the first exon with an *Escherichia coli lacZ* reporter gene. Single- (+/−) and double-targeted (−/−) embryonic stem (ES) clones were obtained at high frequency in two different ES cell lines (*5*, *6*) (Fig. 1A). EGFR$^{-/-}$ ES cells are viable and not impaired in their growth potential (*7*). Several chimeras transmitted the mutated allele to their offspring, and heterozygote mice of both sexes were healthy and fertile (*8*). When inbred 129 EGFR$^{+/-}$ mice were intercrossed, no live −/− offspring were found at embryonic day 12.5 (E12.5) (Table 1). Earlier in their development, mutant embryos were obtained at the expected Mendelian frequency, indicating that implantation and early post-implantation development were not impaired (Table 1). A reduction in the number of live homozygote mutants was observed after E11.5 on a 129 × BL6 background; however, a small number of mutant fetuses developed to term. In a 129 × BL6 × MF1 background, three mutant mice survived until postnatal day 20 (P20) (Table 1). The absence of EGFR mRNA and protein in mutant primary embryonic fibroblasts and E13.5 embryos was confirmed by Northern (RNA) and protein immunoblot analysis (Fig. 1, B and C).

Mutant embryos were slightly reduced in size and weight from E10.5 on a 129 background and from E13.5 on a mixed 129 × BL6 background (Fig. 2A) (*7*). The three 129 × BL6 × MF1 EGFR$^{-/-}$ mice, which survived until P20, were only 40 to 50% of the size and weight of control littermates (*7*). The reduced body weight of the EGFR$^{-/-}$ fetuses was most likely a consequence of the smaller placentas (Fig. 2, A and B). E13.5 mutant placentas were structurally abnormal, and the maternal decidua was more easily separable by manual dissection from the fetal components. The spongiotrophoblast layer was reduced in size, with only a thin layer of *flt-1*– and 4311-expressing spongiotrophoblast cells (Fig. 2, C through E, and G) (*7*, *9*). The labyrinthine trophoblast cells and the network of embryonic vessels and maternal sinuses appeared structurally normal (Fig. 2, C and D), as shown by the expression of *flk-1* in the endothelial cells of the labyrinth (Fig. 2, F and H) (*10*). Secondary giant cells were present in normal numbers and formed multiple cell layers at the interface between the maternal decidua and the embryonic labyrinth (*7*). Thus, the absence of the EGFR appears to specifically affect the proliferation or survival of spongiotrophoblast cells.

Table 1. Viability of offspring from EGFR heterozygote matings in three mouse strains. Genotype analysis of embryos (E9.5 to E18.5), newborn (P1), and adult (P20) offspring from EGFR heterozygote parents in three genetic backgrounds (*8*). After cesarean section, none of the live E18.5 EGFR$^{-/-}$ fetuses sustained respiration for longer than 1 hour, and all 129 × BL6 newborn fetuses (some with milk in their stomachs) died within 12 to 24 hours. Dead EGFR$^{-/-}$ embryos and mice are indicated in squared brackets. +/+, wild-type; +/−, heterozygotes; −/−, homozygote mutants.

Mouse strain	Offspring			Total (litters)
	+/+	+/−	−/−	
E9.5 to 11.5				
129	16	27	12	55 (8)
129 × BL6	31	69	26 [1]	127 (12)
E12.5 to 13.5				
129	26	42	0 [3]	71 (13)
129 × BL6	83	140	43 [8]	274 (37)
E14.5 to 18.5				
129	3	11	0	14 (3)
129 × BL6	94	157	17 [26]	294 (44)
P1				
129 × BL6	44	99	8 [5]	156 (19)
P20				
129; 129 × BL6	104	157	0	261 (31)
129 × BL6 × MF1	281		0 [3]	284 (30)

Research Institute of Molecular Pathology (IMP), Dr. Bohr-Gasse 7, A-1030 Vienna, Austria.

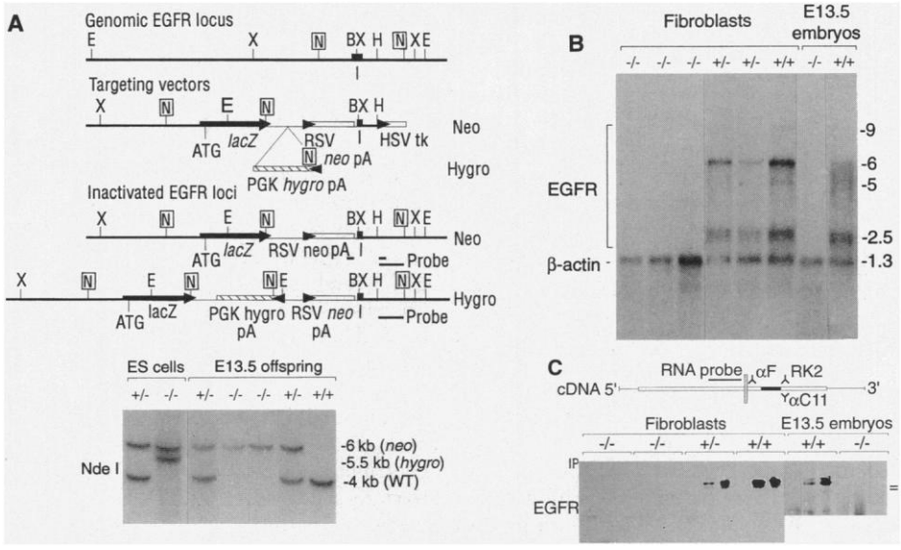

Fig. 1. Disruption of the gene encoding the EGFR in mouse ES cells. (**A**) Restriction map of a 17-kb genomic fragment encompassing promoter regions, the first exon (black box), and part of the first intron are shown in the first line. The second and third lines illustrate the neomycin- (*neo*) and the hygromycin- (*hygro*) targeting vectors, respectively (*5*). Arrowheads depict the promoter position and the transcription orientation of the selection cassettes. The disrupted EGFR alleles are represented in lines 4 and 5. Restriction enzymes: E, Eco RV; X, Xba I; N, Nde I; BX, Bst XI; H, Hind III; __ in line 4 indicates the position of PCR primers (*8*). Southern blot (lower panel) with Nde I digestion [boxed in (A)] and a 3′ external probe detects a 4-kb wild-type (WT) and a 6-kb or 5.5-kb disrupted *neo* and *hygro* allele, respectively. The first two lanes show a single-targeted (+/−) and a double-targeted (−/−) ES cell clone (*6*), and the following lanes the genotypes of a E13.5 progeny from a heterozygote intercross (*8*). (**B**) Expression of EGFR mRNA and β-actin (loading control) in primary embry onic fibroblasts and embryos (*29*). The EGFR cDNA probe used is indicated in the top panel of (C) (*29*). (**C**) Protein immunoblot analysis of immunoprecipitated lysates of primary embryonic fibroblasts and embryos (*30*). EGFR-specific antisera αF (αF) and RK2 (RK) were used for immunoprecipitation and antibody αC11 for immunodetection. The position of the epitopes is indicated in the upper panel. P, preimmune serum; =, 180-kD phosphorylated and unphosphorylated EGFR protein. The absence of EGFR protein was confirmed in an in vitro autophosphorylation assay (*7*).

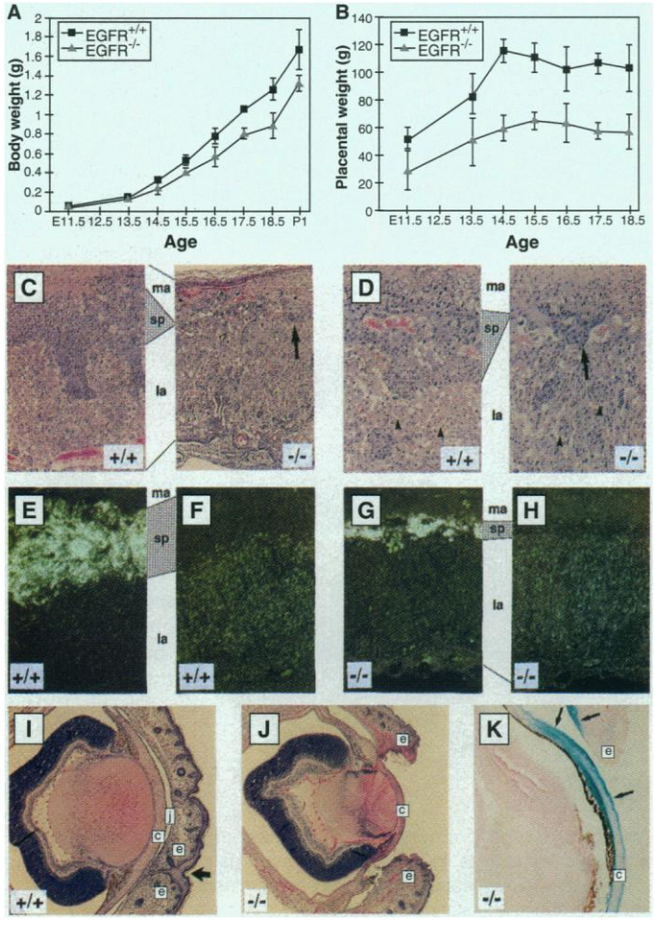

Fig. 2. (**A** and **B**) Growth rates of EGFR$^{+/+}$ and EGFR$^{-/-}$ embryos and placentas. Embryonic (A) and placental (B) weights are shown with embryonic age. The analysis was performed on a mixed 129 × BL6 genetic background, and each stage represents the mean value ± SD of three to seven embryos and placentas. (**C** through **H**) Histological and in situ analysis of E13.5 wild-type and mutant placentas. Sections were stained with hematoxylin-eosin at low (C) and high (D) magnifications. The arrows point to residual spongiotrophoblast cells (sp) in the mutants and arrowheads to labyrinthine trophoblast cells (la). Dark-field images of adjacent +/+ and −/− E13.5 placental sections show the expression of *flt-1* [(E) and (G)] and *flk-1* [(F) and (H)], which are markers for the spongiotrophoblast cells and labyrinthine endothelial cells, respectively. The same phenotype was observed in all mutant placentas analyzed between E11.5 and E18.5 (*7*). ma, maternal decidua. (**I** through **K**) Comparison of frontal sections through the eyes of newborn +/+ (I) and −/− [(J) and (K)] fetuses. The line of fusion between upper and lower eyelid (e) is indicated by an arrow in the +/+ eye. In (K), after X-gal staining expression of the EGFR was detectable in the cell layer at the edges of the eyelids, in the surface epithelium of the cornea, and in the conjunctiva (arrows, blue staining). j, conjunctival sac. Histological sections and in situ hybridization were performed as described (*31*). Magnification: (C), (E) through (J), ×18; (D) and (K), ×35.

At birth, the whiskers of all EGFR$^{-/-}$ fetuses were absent or rudimentary stubs (*7*). After E16.5, surviving mutant fetuses had open eyes (Fig. 2, I through K). Histological analysis of the eyes of mutant newborns showed that the eyelids failed to grow and fuse and that the cornea was thin and fibrotic (Fig. 2, J and K). Because corneal differentiation depends on the formation of the conjunctival sac that occurs after the closure of the eyelids (*11*), it may be that lack of eyelid fusion impaired corneal differentiation. However, the high expression of EGFR [revealed by X-galactosidase (X-gal) staining at the edges of the eyelids and in the corneal epithelium] indicates that receptor expression directly affects the development of these structures (Fig. 2I). Similar malformations with incomplete penetrance were observed in TGF-α$^{-/-}$ and wa-2 mice that have a point mutation in the gene encoding the EGFR that partially impairs receptor signaling (*12*).

Histological analysis of the internal organs of growth-retarded E13.5 mutant embryos showed generalized hypoplasia, but no obvious structural anomalies (*7*). Alterations in the skin were observed in E18.5 and newborn EGFR$^{-/-}$ fetuses. The mutant epidermis was thin, the layers not well distinguished, and keratinization of the stratum corneum was almost absent (Fig. 3, A and B). Expression of the EGFR monitored by X-gal staining was confined to the basal layer of the epidermis (Fig. 3C). In mutants, expression was also detected in the keratinocytes of the suprabasal layers, suggesting an aberrant organization of the epidermis (*7*). At birth, some mutant hair follicles appeared less differentiated, although their number

and organization in the dermal layer were similar to that in the wild type (Fig. 3, A and B). These structures were severely affected in the P20 mutants, which failed to develop a hairy coat (*7*). In contrast, TGF-$\alpha^{-/-}$ and wa-2 mice display waviness of whiskers and fur but normal structure of the epidermis (*12*). These results confirm that EGFR signaling plays an important role in hair follicle and skin development (*12, 13*).

The lungs of E18.5 and newborn EGFR$^{-/-}$ fetuses, which had respired, appeared immature with poorly inflated areas (*7*). Lung sections from these mutants showed undifferentiated epithelium in the respiratory bronchioles and alveoli and increased amounts of cells in the alveolar septae (Fig. 3, D and E). A role for the EGFR in the maturation of the various lung epithelia is supported by X-gal staining in the affected pulmonary cells (Fig. 3F). However, it may be that the immature lungs are a consequence of the growth retardation observed in the mutants.

These defects observed in lung and skin, together with the *lacZ* expression pattern, imply that the EGFR plays an important role in the proliferation and differentiation of the epithelial compartment of these organs. Histological examinations of the epithelial compartments of stomach, small and large intestine, pancreas, liver, kidney, and brain of E18.5 and newborn mutant fetuses revealed no obvious abnormalities (*7*). Surviving P20 mutant mice were severely dehydrated and suffered from a wasting syndrome 2 days before death and exhibited similar histological abnormalities as described by Threadgill *et al.* (*7, 14*).

To assess the proliferation and developmental potential of EGFR$^{-/-}$ cells, we injected three EGFR$^{-/-}$ ES cell clones into wild-type blastocysts to generate chimeras (*6, 7*) (Fig. 4A). All chimeras were alive at E14.5, and efficient ES cell contribution was observed in all embryonic organs analyzed. These chimeras survived longer than inbred 129 EGFR$^{-/-}$ fetuses, most likely because the placenta was mainly derived from host wild-type cells (Fig. 4A) (*15*). At birth, some chimeras had open eyes and contributed fewer EGFR$^{-/-}$ ES cell derivatives to some organs (Fig. 4A). Most chimeras died within a few hours because of an inability to sustain respiration; their phenotype thereby resembled that of newborn mutant fetuses. Those surviving to adulthood contributed few EGFR$^{-/-}$ derivatives to organs like lung, liver, gut, and stomach. In adult chimeras in whom the injected cells were 40 to 50% of skin cells, we could not detect the patchy distribution of wavy and normal hair, which was observed in aggregation chimeras with wa-2/wa-2 embryos (*16*). These results suggest that compared to control cells, EGFR$^{-/-}$ ES cell derivatives might encounter a selective disadvantage in colonizing certain tissues because of a cell-autonomous defect in particular cell lineages.

Altered EGFR signaling has been shown to influence the proliferation and differentiation of hematopoietic cells (*17*). To test whether hematopoiesis was affected, we injected E12.5 mutant fetal liver cells intravenously into wild-type recipient adult mice that were lethally irradiated (*18*). After 8 months, these mice were healthy and the hematopoietic compartment was reconstituted by the mutant cells (Fig. 4B). The number of lymphoid and myeloid cells in the spleen of a mouse reconstituted with EGFR$^{-/-}$ fetal liver cells was comparable to that in the control reconstituted with EGFR$^{+/-}$ cells (Fig. 4B). Interestingly, a reduction in the number of B220^{+} cells was detected in bone marrow. Analysis of peripheral blood showed no significant difference in hematocrits (40 to 50%) and red blood cell counts (8×10^9 to 10×10^9 cells), suggesting that hematopoietic stem cells are functional in EGFR mutant fetal livers.

The placentas of EGFR mutant fetuses are smaller and exhibit an altered spongiotrophoblast layer, the part of the placenta where maternal and fetal tissues come in closest contact. Although the function of the spongiotrophoblast cells is poorly understood (*19*), we speculate that this deficiency is responsible for the altered embryonic-maternal adhesiveness we observed. A role for the EGFR in cell adhesion has indeed been proposed because the EGFR can associate in vitro with the cadherin-catenin complex of transmembrane adhesion molecules (*20*). Altered adhesion might affect placental function, causing growth retardation and subsequent embryonic death. The observation that alterations in the amount of placental EGFR can affect intrauterine growth of human fetuses supports this hypothesis (*21*). In EGFR mouse mutants of 129, 129 × BL6, and 129 × BL6 × MF1 backgrounds, implantation of the blastocyst and further differentiation of the trophectoderm into spongiotrophoblast and labyrinthine trophoblast cells appear to proceed normally; the lack of the EGFR seems to affect only the proliferation or survival of the spongiotrophoblast cells. On the inbred 129 background, EGFR$^{-/-}$ fetuses die around E12.5, which coincides with the stage when correct placental function is required (*3*). Most of the 129 × BL6 mutants also die around E12.5, but some survive with other defects until birth. Because placental development is controlled by several different signaling pathways (*3, 22*), the observation that the number of mutant fetuses surviving after E13.5 is increased when the genetic background is predominantly C57BL/6 (*7*) suggests that these pathways are regulated differently in various mouse strains.

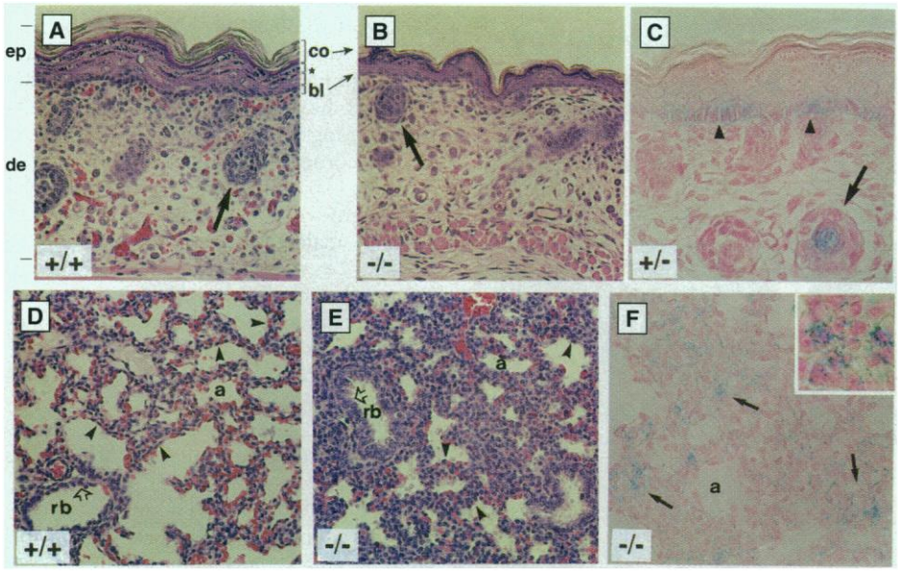

Fig. 3. (**A** through **C**) Sections through the neck skin of wild-type (+/+) (A) and mutant (−/−) (B) newborn and heterozygote (+/−) (C) E18.5 fetuses. Arrows point to the hair follicles. In +/− skin sections X-gal staining is mainly detectable in the basal layer of the epidermis (arrowheads) and in the hair follicles (arrow). ep, epidermis; de, dermis; co, corneal layer; asterisk, granular and spinous layers; bl, basal layer. (**D** through **F**) Comparison of lung sections of E18.5 wild-type (D) and mutant [(E) and (F)] fetuses, which respired and died soon after. The type I pneumocytes that line the alveolar surface are indicated by arrowheads. Open arrows indicate the epithelium of the respiratory bronchioles (rb). These defects were consistently observed in all three E18.5 and five newborn mutant fetuses analyzed. a, alveoli. After X-gal staining, the β-galactosidase activity can be detected in most pneumocytes (arrows and inset) from EGFR −/− and +/− fetuses (F). Magnification: (A), (B), (D) through (F), ×96; (C), ×195; inset in (F), ×488.

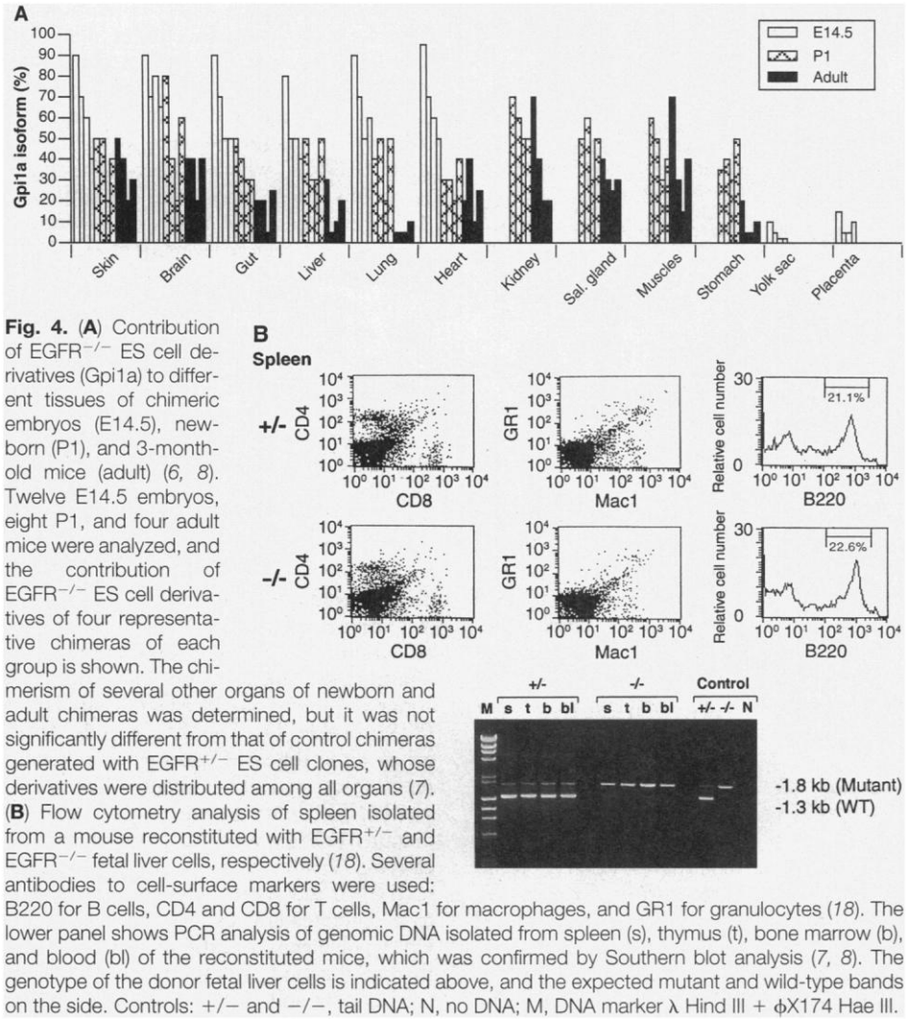

Fig. 4. (**A**) Contribution of EGFR$^{-/-}$ ES cell derivatives (Gpi1a) to different tissues of chimeric embryos (E14.5), newborn (P1), and 3-month-old mice (adult) (*6*, *8*). Twelve E14.5 embryos, eight P1, and four adult mice were analyzed, and the contribution of EGFR$^{-/-}$ ES cell derivatives of four representative chimeras of each group is shown. The chimerism of several other organs of newborn and adult chimeras was determined, but it was not significantly different from that of control chimeras generated with EGFR$^{+/-}$ ES cell clones, whose derivatives were distributed among all organs (*7*). (**B**) Flow cytometry analysis of spleen isolated from a mouse reconstituted with EGFR$^{+/-}$ and EGFR$^{-/-}$ fetal liver cells, respectively (*18*). Several antibodies to cell-surface markers were used: B220 for B cells, CD4 and CD8 for T cells, Mac1 for macrophages, and GR1 for granulocytes (*18*). The lower panel shows PCR analysis of genomic DNA isolated from spleen (s), thymus (t), bone marrow (b), and blood (bl) of the reconstituted mice, which was confirmed by Southern blot analysis (*7*, *8*). The genotype of the donor fetal liver cells is indicated above, and the expected mutant and wild-type bands on the side. Controls: +/− and −/−, tail DNA; N, no DNA; M, DNA marker λ Hind III + ϕX174 Hae III.

REFERENCES AND NOTES

1. C.-H. Heldin, *Cell* **80**, 213 (1995); J. Massagué and A. Pandiella, *Annu. Rev. Biochem.* **62**, 515 (1993); J. Schlessinger and A. Ullrich, *Neuron* **9**, 383 (1992).
2. A. Dardik, R. M. Smith, R. M. Schultz, *Dev. Biol.* **154**, 396 (1992); S. K. Das *et al.*, *Development* **120**, 1071 (1994); L. M. Wiley, J.-X. Wu, I. Harari, E. D. Adamson, *Dev. Biol.* **149**, 247 (1992).
3. J. C. Cross, Z. Werb, S. J. Fisher, *Science* **266**, 1508 (1994).
4. E. D. Adamson, *Curr. Top. Dev. Biol.* **24**, 1 (1990); R. Derynck, *Adv. Cancer Res.* **58**, 27 (1992); A.-M. Partanen, *Curr. Top. Dev. Biol.* **24**, 31 (1990).
5. EGFR complementary DNA (cDNA) (first exon) (*23*) was used to screen a Lambda FIX II 129/Sv genomic library (Stratagene). For the neomycin-targeting vector, a 5.0-kb Xba I–Nae I genomic fragment encompassing the 5′ promoter region and untranslated parts of the first exon was cloned into the Xba I and Xmn I sites of pGNA (*24*). A 0.95-kb Bst XI–Hind III 3′ region and a 1.8-kb gene encoding herpes simplex virus–thymidine kinase with its own promoter and polyadenylate [poly(A)] site were inserted into the Sma I and Asp^{718} sites, respectively. The hygromycin-targeting vector was modified from the neomycin-targeting vector by introduction of a 2-kb Cla I–Xho I phosphoglycerate kinase–hygromycin fragment (*25*) into the Sal I site of pGNA. In both constructs, 117 bp of the first exon including the EGFR translation initiation site and parts of the leader peptide (amino acids 1 to 13), which is responsible for targeting the receptor protein to the cell surface, were deleted and replaced by the *lacZ* gene with its own ATG (*24*). Therefore, in the targeted alleles *lacZ* expression should be regulated by the endogenous EGFR promoter.
6. The neo-targeting vector was linearized with Xba I and electroporated into feeder-dependent D3 (*25*) and R1 ES cells (*26*). Selection and screening of ES cell colonies by the polymerase chain reaction (PCR) was performed with two sets of nested primers as described (*25*), and correct targeting was confirmed by Southern (DNA) blot analysis with Eco RV, Xba I, and Nde I and a Hind III–Nae I 3′ end probe, external to the targeting vector. An internal probe was used to verify that no additional rearrangements or random integrations had occurred. The frequency of homologous recombination was 1 in 12 for D3 ES cells and 1 in 5 for R1 ES cells. The A4 clone of R1 EGFR$^{+/-}$ ES cells (R1.A4) was electroporated with the Xba I–linearized, *hygro*-targeting vector to generate double-targeted EGFR$^{-/-}$ ES cells, which were obtained at a frequency of 1 in 12.
7. M. Sibilia and E. F. Wagner, data not shown.
8. Chimeric mice were generated by microinjection of D3.D1, R1.A4, and R1.C8 EGFR$^{+/-}$ ES cells into C57BL/6 blastocysts (*6*). Several chimeric males generated with all three clones and one female transmitted the targeted EGFR allele to their offspring. Chimeras were mated to 129/Sv or C57BL/6 females to obtain EGFR$^{+/-}$ offspring of inbred 129 and mixed 129 × BL6 genetic background. EGFR$^{+/-}$ 129 × BL6 mice were mated to MF1 to obtain the mixed 129 × BL6 × MF1 background. Heterozygotes were further intercrossed to generate mice homozygous at the EGFR locus. DNA was prepared from yolk sacs or tails and genotyped by Southern blotting or PCR as described (*25*). Primer positions for amplification of wild-type and mutated alleles are indicated in Fig. 1A. For the generation of chimeras with EGFR$^{-/-}$ ES cells, clones A4, C4, and D7, derived from clone R1.A4 (*6*), were injected into C57BL/6 blastocysts. Organs were analyzed for glucose phosphate isomerase (Gpi) isoenzyme distribution as described (*25*). The contribution was determined by visual comparison of the intensity of the Gpi1a (from the 129/Sv ES cells) versus that of the Gpi1b (from the C57BL/6 host blastocyst) bands on a cellugel (*25*). The chimerism in adult skin was judged by coat color (agouti versus black fur).
9. H. Finnerty *et al.*, *Oncogene* **8**, 2293 (1993); K. R. Lescisin, S. Varmuza, J. Rossant, *Genes Dev.* **2**, 1639 (1989).
10. G. Breier, M. Clauss, W. Risau, *Dev. Dynamics*, in press.
11. M. H. Kaufman, in *The Atlas of Mouse Development*, M. H. Kaufman, Ed. (Academic Press, London, 1992), p. 407.
12. K. J. Fowler *et al.*, *Proc. Natl. Acad. Sci. U.S.A.* **92**, 1465 (1995); N. C. Luetteke *et al.*, *Cell* **73**, 263 (1993); N. C. Luetteke *et al.*, *Genes Dev.* **8**, 399 (1994); G. B. Mann *et al.*, *Cell* **73**, 249 (1993).
13. A. M. Dominey *et al.*, *Cell Growth Differ.* **4**, 1071 (1993); R. Vasser and E. Fuchs, *Genes Dev.* **5**, 714 (1991).
14. D. W. Threadgill *et al.*, *Science* **269**, 230 (1995).
15. R. S. P. Beddington and E. J. Robertson, *Development* **105**, 733 (1989).
16. A. McLaren and P. Bowman, *Nature* **224**, 238 (1969).
17. M. J. Hayman, S. Meyer, F. Martin, P. Steinlein, H. Beug, *Cell* **74**, 157 (1993); B. Pain *et al.*, *ibid.* **65**, 37 (1991); T. von Rüden, S. Kandels, T. Radaszkiewicz, A. Ullrich, E. F. Wagner, *Blood* **12**, 3145 (1992).
18. Fetal liver cells isolated from 129 × BL6 E12.5 +/− and −/− embryos were resuspended in phosphate-buffered saline (PBS), and 10^6 cells were injected intravenously into adult 129 × BL6 wild-type recipient mice that were lethally irradiated (9.5 Gy). All control mice injected with PBS died after 2 weeks. After 8 months, the hematopoietic compartments of the reconstituted mice were analyzed by FACScan with different cell surface markers as described (*25*).
19. M. Müntener and Y.-C. Hsu, *Acta Anat.* **98**, 241 (1977); J. Rossant and B. A. Croy, *J. Embryol. Exp. Morphol.* **86**, 177 (1985).
20. H. Hoschuetzky, H. Aberle, R. Kemler, *J. Cell Biol.* **127**, 1375 (1994).
21. C. Fondacci *et al.*, *J. Clin. Invest.* **93**, 1149 (1994).
22. F. Guillemot, A. Nagy, A. Auerbach, J. Rossant, A. L. Joyner, *Nature* **371**, 333 (1994); C. Schmidt *et al.*, *ibid.* **373**, 699 (1995); Y. Uehara *et al.*, *ibid.* **373**, 702 (1995).
23. A. Avivi *et al.*, *Oncogene* **6**, 673 (1991).
24. H. Le Mouellic, Y. Lallemand, P. Brûlet, *Cell* **69**, 251 (1992).
25. F. Hilberg, A. Aguzzi, N. Howells, E. F. Wagner, *Nature* **365**, 179 (1993); P. Urbanek, Z.-Q. Wang, I. Fetka, E. F. Wagner, M. Busslinger, *Cell* **79**, 901 (1994).
26. A. Nagy, J. Rossant, R. Nagy, W. Abramow-Newerly, J. Roder, *Proc. Natl. Acad. Sci. U.S.A.* **90**, 8424 (1993).
27. N. Redemann *et al.*, *Mol. Cell. Biol.* **12**, 491 (1992).
28. D. G. Wilkinson, J. A. Bailes, J. E. Champion, A. P. MacMahon, *Development* **99**, 493 (1987).
29. Poly(A)$^+$ RNA was isolated from E13.5 embryos and primary embryonic fibroblasts, and Northern (RNA) blots were analyzed by hybridization with an Eco RI, Hinc II–Eco RI extracellular (*23*), and Eco RI intracellular (*12*) mouse EGFR cDNA fragment (*25*).
30. EGFR antibodies were RK2 and αF rabbit antisera directed against residues 984 to 996 and 656 to 676 and αC11 mouse monoclonal antibody directed against residues 996 to 1022 (Transduction Laboratories). Cell and embryo lysates were processed as described (*27*). Protein quantified by the Bradford method, immunoprecipitation, SDS–polyacrylamide gel electrophoresis, and protein immunoblot analysis were as described (*27*).
31. Organs and fetuses were fixed in 4% paraformaldehyde and embedded in paraffin. Sections (5 μm) were stained with hematoxylin-eosin (*25*) or pro-

cessed for mRNA in situ hybridization with *4311*, *flt-1*, and *flk-1* riboprobes as described (*28*). Embryos or organs were stained with X-gal as described (*25*), and no background staining was detected in all control tissues. Sections were counterstained with nuclear red.

32. We are grateful to I. Fetka and U. Möhle-Steinlein for technical assistance; N. Howells and C. Theussl for maintaining our mouse colony; A. Aguzzi, K. Zatloukal, and F. Guillemot for advice on pathology; P. Steinlein for help with FACScan analysis; R. Kurzbauer for DNA sequencing; F. Guillemot and W. Risau for providing the *4311*, *flk-1*, and *flt-1* plasmids; J. Schlessinger for the EGFR antibodies; M. Oft and all the members of the Wagner lab for helpful discussions; A. Aguzzi, D. Barlow, H. Beug, A. Grigoriadis, and Z-Q. Wang for critical reading of the manuscript; and H. Tkadletz for prepairing the illustrations. M.S. was a recipient of a fellowship from Associazione Italiana per la Ricerca sul Cancro (AIRC). Supported in part by the Austrian Industrial Research Promotion Fund.

7 April 1995; accepted 23 June 1995

Requirement of the Yeast *RTH1* 5′ to 3′ Exonuclease for the Stability of Simple Repetitive DNA

Robert E. Johnson, Gopala K. Kovvali, Louise Prakash, Satya Prakash*

Simple repetitive DNA sequences are unstable in human colorectal cancers and a variety of other cancers. Mutations in the DNA mismatch repair genes *MSH2, MLH1,* and *PMS1* result in elevated rates of spontaneous mutation and cause a marked increase in the instability of simple repeats. Compared with the wild type, a null mutation in the yeast *RTH1* gene, which encodes a 5′ to 3′ exonuclease, was shown to increase the rate of instability of simple repetitive DNA by as much as 280 times and to increase the spontaneous mutation rate by 30 times. Epistasis analyses were consistent with the hypothesis that this *RTH1*-encoded nuclease has a role in the *MSH2-MLH1-PMS1* mismatch repair pathway.

Defects in DNA mismatch repair in *Escherichia coli* and yeast result in an increase in the instability of simple repetitive DNA sequences (*1*, *2*). Tumors from hereditary nonpolyposis colorectal cancer (HNPCC) kindreds contain frequent alterations in the length of microsatellites (*3*), and mutations in any of the four known human mismatch repair genes, *hMSH2*, *hMLH1*, *hPMS1*, and *hPMS2*, are associated with most of these cancers (*4*, *5*). HNPCC patients account for 3 to 6% of colorectal cancers each year (*6*). Colorectal cancers also occur in patients without a strong family history of the disease, and these too display microsatellite instability (*3*, *5*, *7*). However, a large proportion of the sporadic tumor cell lines with microsatellite instability do not contain mutations in the four mismatch repair genes, which suggests that other genes may contribute to microsatellite instability and cancer (*5*).

In eukaryotes, long-patch DNA repair of both base mismatches and loops has bidirectional excision capability (*8*); hence, 5′ to 3′ and 3′ to 5′ exonucleases may play a role in the repair process. The *RTH1* gene of *Saccharomyces cerevisiae* encodes the yeast counterpart of the mammalian 45-kD 5′ to 3′ exonuclease required for lagging-strand DNA synthesis in reconstituted systems (*9*, *10*). After the ribonuclease H1–catalyzed cleavage of primer RNA one nucleotide 5′ of the RNA-DNA junction, the 5′ to 3′ exonuclease removes the remaining monoribonucleotide of the RNA primer (*10*). A null mutation of *RTH1* (*rth1*Δ) causes conditional lethality at 37°C; mutant cells are blocked in nuclear division and have a morphology typical of mutants defective in DNA replication. At the permissive temperature, rates of spontaneous mitotic recombination are elevated in the *rth1*Δ strain, and sensitivity to the alkylating agent methyl methanesulfonate is enhanced (*9*). Here, we show that the *rth1*Δ mutation increases the instability of simple repetitive sequences.

Poly(GT) repeat sequences ranging in size from 10 to 30 repeats are present in most eukaryotes, including humans (*11*). To examine the effect of *RTH1* on the stability of poly(GT) repeats, we used two types of low-copy centromeric plasmids. Plasmid pSH91 contains an in-frame 33–base pair (bp) poly(GT)$_{16}$G insertion within the coding sequence of a modified *URA3* gene (*2*). Alterations of the tract that produce an out-of-frame mutation produce Ura$^-$ cells that are resistant to 5-fluoroorotic acid (5-FOA). Plasmid pSH31 contains an out-of-frame 29-bp poly(GT)$_{14}$G insertion within the coding sequence of the β-galactosidase gene (*12*). Alterations of the tract that restore the correct frame produce blue colonies on medium containing X-Gal (5-bromo-4-chloro-3-indolyl-β-D-galactopyranoside). To monitor frame shifting within the chromosome, we used yeast strain SH75, in which an out-of-frame 29-bp poly(GT)$_{14}$G sequence containing a β-galactosidase construction similar to that in pSH31 has been integrated into the yeast genome at the *LYS2* locus (*12*).

The *rth1*Δ mutation increased tract instability in all three systems. In the two plasmid-based systems, we observed rates of tract alteration in the *rth1*Δ mutant that were 100 to 280 times the wild-type rate (Table 1). Tract instability within the chromosome also increased in the *rth1*Δ strain, but its magnitude (43 times the wild-type rate) was less than that in the plasmid systems. This result is consistent with the observation that tract instability is less pronounced in the chromosome than in the plasmids in the *pms1* mutant (*2*) (Table 1). The rate of tract alteration in the *rth1*Δ strain was one-half to one-third the rate in the isogenic strains that contained mutations in *MSH2*, *MLH1*, or *PMS1* (Table 1). The *PMS1* and *MLH1* genes act in the same pathway of mismatch repair, because double mutants show microsatellite instability similar to that of single mutants (*2*). Conversely, a double mutant carrying a *pms1* mutation in combination with a *pol2* mutation, which abolishes the 3′ to 5′ proofreading exonuclease activity of DNA polymerase ε, exhibits mutation rates that are the product of the relative mutation rates of *pol2* and *pms1* single mutants (*13*); this finding indicates that mismatches that accumulate in the absence of *POL2* proofreading activity are removed by the mismatch repair system.

To determine whether *RTH1* functions in concert with *MSH2*, *MLH1*, and *PMS1*, we examined tract instability in the double mutants *rth1*Δ*msh2*Δ, *rth1*Δ*mlh1*Δ, and *rth1*Δ*pms1*Δ. We found that the *rth1*Δ mutation in combination with any of the mismatch repair mutations resulted in rates of tract instability that were about three times those of isogenic strains defective in a single mismatch repair gene. These observations suggest that in addition to playing a role in the *MSH2-MLH1-PMS1* mismatch repair pathway, *RTH1* effects mismatch removal by another minor repair pathway.

Previous studies have suggested that the *MSH2-MLH1-PMS1* pathway of mismatch repair primarily corrects insertions or deletions of one or two units of dinucleotide repeats (*2*). To determine the types of repeat alterations generated in the *rth1*Δ strains, we sequenced plasmid DNA that contained tract alterations from 5-FOA–resistant colonies or from blue colonies on X-Gal plates (Table 2). With the exception

Sealy Center for Molecular Science, University of Texas Medical Branch, 6.104 Medical Research Building, 11th and Mechanic Streets, Galveston, TX 77555–1061, USA.

*To whom correspondence should be addressed.